Biochimica et Biophysica Acta xxx (2016) xxx–xxx

Contents lists available at ScienceDirect

Biochimica et Biophysica Acta

journal homepage: www.elsevier.com/locate/bbapap

Molecular profiles of thyroid cancer subtypes: Classification based on features of tissue revealed by mass spectrometry imaging

Monika Pietrowska [a], Hanna C. Diehl [b], Grzegorz Mrukwa [c], Magdalena Kalinowska-Herok [a], Marta Gawin [a], Mykola Chekan [a], Julian Elm [b], Grzegorz Drazek [c], Anna Krawczyk [c], Dariusz Lange [a], Helmut E. Meyer [b,d], Joanna Polanska [c,*], Corinna Henkel [b,d,**], Piotr Widlak [a,*]

[a] Center for Translational Research and Molecular Biology of Cancer, Maria Sklodowska-Curie Memorial Cancer Center and Institute of Oncology Gliwice Branch, ul. Wybrzeze Armii Krajowej 15, 44101 Gliwice, Poland
[b] Medizinisches Proteom-Center, Ruhr-University Bochum, Universitätsstraße 150, 44801 Bochum, Germany
[c] Faculty of Automatic Control, Electronics and Computer Science, Silesian University of Technology, ul. Akademicka 16, 44100 Gliwice, Poland
[d] Leibniz-Institut für Analytische Wissenschaften - ISAS - e.V., Bunsen-Kirchhoff-Straße 11, 44139 Dortmund, Germany

ARTICLE INFO

Article history:
Received 23 June 2016
Received in revised form 7 October 2016
Accepted 11 October 2016
Available online xxxx

Keywords:
Classification
FFPE tissue
Mass spectrometry imaging
Molecular signature
Thyroid cancer

ABSTRACT

Determination of the specific type of thyroid cancer is crucial for the prognosis and selection of treatment of this malignancy. However, in some cases appropriate classification is not possible based on histopathological features only, and it might be supported by molecular biomarkers. Here we aimed to characterize molecular profiles of different thyroid malignancies using mass spectrometry imaging (MSI) which enables the direct annotation of molecular features with morphological pictures of an analyzed tissue. Fifteen formalin-fixed paraffin-embedded tissue specimens corresponding to five major types of thyroid cancer were analyzed by MALDI-MSI after in-situ trypsin digestion, and the possibility of classification based on the results of unsupervised segmentation of MALDI images was tested. Novel method of semi-supervised detection of the cancer region of interest (ROI) was implemented. We found strong separation of medullary cancer from malignancies derived from thyroid epithelium, and separation of anaplastic cancer from differentiated cancers. Reliable classification of medullary and anaplastic cancers using an approach based on automated detection of cancer ROI was validated with independent samples. Moreover, extraction of spectra from tumor areas allowed the detection of molecular components that differentiated follicular cancer and two variants of papillary cancer (classical and follicular). We concluded that MALDI-MSI approach is a promising strategy in the search for biomarkers supporting classification of thyroid malignant tumors. This article is part of a Special Issue entitled: MALDI Imaging, edited by Dr. Corinna Henkel and Prof. Peter Hoffmann.

1. Introduction

Thyroid nodules are very common in the general population and can be detected by palpation or ultrasonographic survey in about 5% of the adult population. Malignant tumors occur in 5–10% of such nodules, hence thyroid cancer is the most common endocrine malignancy and comprises 1–3% of all cancers worldwide [1]. The majority of thyroid carcinomas originate from follicular epithelial cells and include well-differentiated papillary thyroid carcinomas (PTC; >70% of all thyroid malignancies) and follicular thyroid carcinomas (FTC; 10–20% of thyroid malignancies), as well as anaplastic (undifferentiated) carcinomas (ATC) which are the most aggressive thyroid malignancy (1–2% of thyroid cancers); moreover, two variants of PTC can be distinguished: classical (PTC-CV) and follicular (PTC-FV). Furthermore, medullary thyroid carcinoma (MTC) that is derived from the parafollicular C-cells and has neuroendocrine features, comprises 3–5% of thyroid cancers. The types of thyroid cancer are distinguished based on histopathological features, and this classification is the primary step in the assessment of prognosis and selection of a treatment [2–5]. The majority of patients with thyroid cancer are initially diagnosed based on the fine needle aspiration cytology (FNAC) of thyroid nodules [6,7]. Further diagnosis is performed based on a histopathological intraoperative examination of the resected thyroid tissue. However, in some cases cytological and histological patterns are ambiguous and proper classification is problematic [8]. For example, among important challenges in the diagnostics of thyroid cancer there is differentiation between benign follicular

* Corresponding authors.
** Correspondence to: C. Henkel, Medizinisches Proteom-Center, Ruhr-University Bochum, Universitätsstraße 150, 44801 Bochum, Germany.
E-mail addresses: joanna.polanska@polsl.pl (J. Polanska), corinna.henkel@isas.de (C. Henkel), piotr.widlak@io.gliwice.pl (P. Widlak).

http://dx.doi.org/10.1016/j.bbapap.2016.10.006
1570-9639/

adenoma, follicular carcinoma and the follicular variant of papillary carcinoma, which share several histological features [9,10].

Currently, classification of thyroid cancer based on histopathological patterns could be supported by molecular biomarkers, including markers identified with the use of high-throughput "omics" approaches [11–16]. The most numerous and advanced studies are based on mutation and gene expression profiling. This type of studies revealed several gene expression signatures, some of them associated with mutations in cancer driver genes, which enable us to distinguish different types of thyroid cancers or malignant tumors from benign lesions [17–21]. A few proteomics studies also identified proteins whose differential abundances could allow the discrimination of cancerous and normal thyroid tissue [22,23], malignant and benign follicular lesions [24,25], or papillary and follicular cancers [26]. Similarly, metabolomics analysis of thyroid tissue could also reveal molecular signatures characteristic for different types of thyroid lesions [27]. It is noteworthy, however, that the presence of non-tumor tissue in analyzed material can markedly affect composition and performance of molecular signatures built for the classification of thyroid lesions. Therefore, performing molecular analysis using micro-dissected material should always be considered [28]. Moreover, molecular intra-tumor heterogeneity is still a rather underresearched aspect in the thyroid cancer field [29]. Hence, the direct combination of knowledge of molecular profiles with morphological features of an analyzed tissue would be a valuable approach in the search for molecular classifiers of thyroid tumors.

Mass spectrometry imaging (MSI) is an emerging approach in biomedical research and it is recently evolving into a powerful tool in the study of various types of diseases. The major benefit of MSI is the possibility to combine molecular and morphological information, since molecular images are spatially resolved and well-correlated with the respective histological images. Moreover, different molecular species, e.g. proteins, peptides, lipids, drugs and their metabolites can be imaged, significantly broadening the amount of information derived from a tissue [30–33]. Among many applications of MSI there was molecular characterization and classification of different types of solid tumors [34–38]. The particular advantage of MSI in cancer research is the allocation of molecular profiles to specific cell types, such as cancerous, preneoplastic or inflammatory. Moreover, MSI could be used in the studies of the interface of tumor and normal tissue (tumor niche) and intra-tumor heterogeneity [39–44]. In recent years there were also a few attempts to implement MSI in the studies of thyroid cancer. MSI analysis of cytological material from FNA biopsies revealed proteomic profiles characteristic for different types of thyroid cancer [45–46]. Recently Pagni et al. showed that MALDI-MSI was capable of distinguishing between papillary thyroid cancer and benign thyroid tumors using proteomic signatures of cytological samples [47]. Furthermore, MSI analysis of thyroid tissue allowed detection of proteins discriminating papillary cancer from normal thyroid [48]. Hence, these preliminary studies indicated the promising potential of the MSI approach in the search for molecular signatures that could be used in the classification of thyroid malignancies. Here, we aim to use MALDI-MSI to identify cancer type-specific features of formalin-fixed paraffin-embedded (FFPE) tissue samples representative for five types of thyroid cancers, and to apply molecular signatures revealed by MSI for classification of malignant tissue specimens. Furthermore, we established and implemented an original semi-supervised approach to the detection of the cancer region of interest (ROI).

2. Methods

2.1. Clinical material

Postoperative tissue collected during thyroidectomy and stored as formalin-fixed paraffin-embedded material was used in the study. Tissue samples represented five types of thyroid malignancies: anaplastic thyroid carcinoma (ATC), follicular thyroid carcinoma (FTC), classic variant of papillary thyroid carcinoma (PTC-CV), follicular variant of papillary thyroid carcinoma (PTC-FV), and medullary thyroid carcinoma (MTC); the material was collected from three patients in each group (Table 1 presents detailed description of the clinical material). Thyroidectomy was performed between 1996 and 2011 at Maria Skłodowska-Curie Memorial Cancer Center and Institute of Oncology in Gliwice. The study was approved by the Institutional Ethics Committee (Approval No. KB/430-49/12). Tissue material was re-inspected by an experienced pathologist before the study; the selected samples contained 50–90% of cancer tissue (small amounts of normal thyroid, muscles and connective tissue were also present).

2.2. Sample preparation

FFPE tissue samples were sectioned (10 μm) using a rotary microtome (HM 340E, Thermo Fisher Scientific, Waltham, MA, USA) at room temperature and placed on ITO coated glass slides (Bruker Daltonik, Bremen, Germany). Tissue sections were subjected to dewaxing and rehydration in histology glass containers via consecutive washes (5 min each) in: xylene (twice), isopropanol, ethanol 99.8%, 90%, 70% and 50% EtOH, and finally in TBS buffer. The rehydration step was followed by heat-induced antigen retrieval: sections were heated at 97 °C for 30 min in a retrieval solution (20 mM Tris/EDTA buffer, pH 9). In the next step tissue sections were coated with a solution of trypsin (20 μg in 200 μL of 50 mM NH_4HCO_3; Promega, Madison, USA) with the use of an automatic spraying device (ImagePrep, Bruker), then incubated for 18 h at 37 °C in a humid chamber. Optical images were registered (1200 dpi), and then samples were coated with methanolic solution of 2,5-dihydroxybenzoic acid (50% methanol, 30 mg/mL DHB, 1% TFA). The matrix was deposited using ImagePrep device with Bruker's standard matrix coating program with doubled phase 5 (DHB_for_Digest_nsh01).

2.3. MALDI imaging

Matrix-coated sections were subjected to imaging with the use of a MALDI-TOF/TOF ultrafleXtreme (Bruker) spectrometer equipped with a smartbeam II™ laser operating at 1 kHz repetition rate. Ions were accelerated at 25 kV with PIE time of 100 ns. Spectra were recorded in positive reflectron mode within m/z range of 600–4000 and externally calibrated with Peptide Calibration Standard II (Bruker). A raster width of 100 μm was applied with a large laser focus and 500 shots were collected from each ablation point (random walk was activated in the scanning procedure with 50 shots at a raster spot). Compass 1.4 for FLEX series (Bruker) was employed for spectra acquisition,

Table 1
Description of clinical material.

Code	Pathology	Stage	Sex	Age	Surgery	Content
MTC-1	MTC	pT1bN1bMx	M	47	2003	C, T
MTC-2	MTC	pT2N0Mx	M	51	2004	C, T, F
MTC-3	MTC	pT2(m)N1bMx	M	60	2006	C, T, F
ATC-1	ATC	pT4bN1bMx	F	75	2002	C, N
ATC-2	ATC	pT4bN1aMx	M	62	2004	C, N
ATC-3	ATC	pT4aN1bMx	M	14	2000	C, N, T
FTC-1	FTC	pT1bNxMx	F	65	1999	C, F
FTC-2	FTC	pT3N0Mx	M	57	1996	C, F
FTC-3	FTC	pT2NxMx	F	44	2011	C, F
PTC_CV-1	PTC CV	pT2N1aMx	F	58	2004	C, M, A, F
PTC_CV-2	PTC CV	pT1bNxMx	M	67	2002	C, M, A, F
PTC_CV-3	PTC CV	pT3(m)NxMx	F	64	2002	C, T, M, F
PTC_FV-1	PTC FV	pT2N1bMx	M	20	2003	C, M, A, F
PTC_FV-2	PTC FV	pT2N1aMx	F	31	2004	C, T, F
PTC_FV-3	PTC FV	pT1bN1bMx	M	9	2000	C, A, F

Pathology: MTC — medullary thyroid carcinoma; ATC — anaplastic thyroid carcinoma; FTC — follicular thyroid carcinoma; PTC_CV — papillary thyroid carcinoma, classic variant; PTC_FV — papillary thyroid carcinoma, follicular variant; patient's sex: F — female, M — male; tissue sample content: C — carcinoma, N — necrosis, T — normal thyroid, M — muscle, A — adipose tissue, F — fibrous tissue.

Please cite this article as: M. Pietrowska, et al., Molecular profiles of thyroid cancer subtypes: Classification based on features of tissue revealed by mass spectrometry imaging, Biochim. Biophys. Acta (2016), http://dx.doi.org/10.1016/j.bbapap.2016.10.006

processing and creation of molecular images. After imaging the matrix was washed off the glass slides with 70% ethanol (two washes, 1 min each) and the sections were stained with hematoxylin and eosin, then scanned and used for image co-registration using flexImaging version 4.1 software (Bruker).

2.4. Spectra processing and identification of spectral components

Spectrum preprocessing included resampling to common *m/z* channels followed by detection and removal of a baseline (baseline detection employed the envelope spanned over 10% intensity quantiles calculated for every 200 *m/z* windows approximated with the use of spline technique). The spectra were then aligned, TIC normalized and averaged over all preparations. The mean spectrum was decomposed into Gaussian Mixture Model (GMM) as described in detail elsewhere [49]; the model components were used to define spectral features. For every specific (x,y) point in every preparation and for every component in GMM model a convolution of a normalized MALDI spectrum and a component of Gaussian function was performed giving an integral of the pointwise multiplication of these two functions as the GMM component-related feature value.

2.5. Deglomerative ik-means based grouping of tissue preparations

GMM-based features were used during the iterative divisive ik-means segmentations (DivIK) of all 15 samples together according to the approach described in detail elsewhere [50]. The feature abundance filtering [51] was applied to remove peptides with intensities at the noise level. During each iteration of the developed algorithm, the most informative features within a tissue region (cluster) were identified with the use of the same filtration technique, yet signal decomposition was performed in the domain of variance of peak abundance across the cluster. K-means algorithm with intelligent setting of initial conditions (named *ik-means*) was applied in the stepwise splitting. Dunn's index was used to decide on the number of clusters in a particular splitting. During the succeeding steps, each cluster found in the previous step was split independently of the others. The splitting was performed till the cluster's size (measured by the number of spectra included) reached a priori assumed limit of 0.1% of the original number of (x,y) points in the dataset or the third level of splitting was achieved. The obtained clusters were then characterized by their centroids calculated over all GMM-based features. The final set of centroids, representing molecularly homogenous regions within tissue sample, was then used in further analyses. After each step of the deglomerative segmentation, cluster enrichment analysis was performed within each sample allowing the identification of clusters over represented in particular samples. X^2 test of independence was applied to verify the hypothesis. If any outlying group of such samples was found, it was excluded from the next step of splitting.

2.6. Step-down segmentation and expanded ROI

The DivIK-based step-down segmentation of data was performed for each sample separately to obtain basic (core) homogenous segments further represented by their centroids. The algorithm's stop criterion was related to cluster size only, i.e. 0.1% of original number of spectra in the sample. The correlation-based dissimilarity index was estimated between each basic segment and a sample-specific expert-defined cancer reference area. The distribution of such dissimilarity indices was subjected to the Gaussian Mixture Modeling [51], which allowed the estimation of the dissimilarity thresholds separating groups of segments that were the most similar and the most dissimilar to the reference area. Segments allocated to the "cancer-similar" group constructed the cancer "extended Region of Interest" (exROI).

2.7. Cancer classification

The initial set of 15 samples was randomly split into two balanced subsets: training and testing ones — the random drawing was done independently for each cancer type keeping 2:1 ratio between training and testing sets. Two classification approaches were compared.

2.7.1. Classical approach

The training dataset included 58,890 spectra from the tumor regions manually segmented by an expert (supervised approach); each spectrum was labeled with a cancer type. Five "One (cancer type) versus Other (cancer types)" (OvO) binary classifiers were built using the logistic regression framework with Bayes factor as a criterion for model selection. The value of Bayes factor showing at least strong evidence ($BF > 10^{3/2}$) was set as the inclusion criterion in the forward stepwise procedure of model construction. The regression models were then applied to calculate the probability that a particular "cancerous" spectrum belonged to a particular cancer type; the spectrum was classified as "belonged to cancer type" if the calculated probability was >0.5. The maximum probability criterion was applied, where the type of tested sample is enforced by the leading cancer type assigned to the spectra within the tumor region. Only samples with >50% of spectra being of the same type were classified (others were labeled as "undetermined"). The performance of the obtained classifiers was checked using the training and testing sample sets.

2.7.2. Novel approach

Cancer exROIs and corresponding "Not Cancer" exROIs from 10 training samples (semi-supervised approach) defined the starting training data set, and were used to build the "Cancer versus Not Cancer" (CvNC) binary classifier. The classifier training was performed in the domain of 2478 homogenous similar-to-cancer basic segments, each represented by its centroid calculated in the domain of 3216 GMM components. The logistic regression framework with all the settings similar to those from classical approach was applied. The obtained regression model was then applied to calculate the probability of spectrum to be cancer-similar: the spectrum was classified as "actual cancer" if the estimated probability was >0.5. Together with the CvNC classifier, five additional "One versus Others" (OvO) binary classifiers were also built using the same framework. The performance of the obtained classifiers was checked using the training and testing sample sets. Additional set of 4 new samples was included for the independent validation of the OvO classifiers. In contrary to samples from the testing set, these samples were not considered while the GMM model was built. The raw spectra from the independent validation set were aligned to the average spectrum of the initial 15 samples and normalized to their average TIC value, then the components' abundances were found by the convolution of 3216 GMM masks. Two steps of classification were performed: during the first one "actual cancer" spectra were found with the use of general CvNC classifier. The second step employed all five OvO classifiers to predict the cancer type of all cancer spectra.

2.8. Supervised detection of GMM-based components differentiating between types of cancer

Both expert-defined cancer regions and cancer exROIs were used in the search for GMM-based components discriminating between the types of cancer. Components that putatively corresponded to four major tryptic fragments of trypsin, namely 842.51, 1045.56, 2211.10 and 2283.18 Da, were removed from the analysis. Parametric Tukey-Kramer tests were applied to verify hypotheses on equality of abundance level of spectral components between cancer types. The conservative Bonferroni correction for multiple testing together with additional condition on large effect size measured by the Cohen's d statistics to be higher than 0.8 were applied to avoid large false discovery rates.

Please cite this article as: M. Pietrowska, et al., Molecular profiles of thyroid cancer subtypes: Classification based on features of tissue revealed by mass spectrometry imaging, Biochim. Biophys. Acta (2016), http://dx.doi.org/10.1016/j.bbapap.2016.10.006

2.9. Hierarchical agglomerative clustering of ik-means centroids and mean spectra

The centroids of the 3rd level clusters obtained in global divisive ik-means-based segmentation were subjected to agglomerative merging by hierarchical clustering technique with average linkage function and Pearson's correlation coefficient serving as a similarity measure. Similar hierarchical agglomeration was done in the domain of average GMM-based features (the mean spectra).

3. Results

There were fifteen FFPE tissue specimens representative for five types of thyroid cancer, namely medullary (MTC), anaplastic (ATC) and three types of differentiated cancers (FTC, PTC-CV and PTC-FV) (Table 1), analyzed by MALDI-MSI. The selected specimens mostly comprised of cancerous tissue and a minor proportion of other tissues (normal thyroid, muscles and connective tissue), which was verified by an experienced pathologist based on histological features. Tissue samples were analyzed after in-situ trypsin digestion within 600–4000 Da mass range, hence the majority of detected components (with masses above 800 Da) corresponded to tryptic fragments of proteins present in cancer tissue (including their isotopic envelope). There were 3216 components identified, which comprehensively described molecular profiles of all analyzed tissue samples. Complete information about the abundance of these components was used in both supervised and unsupervised analyses aimed at the estimation of differences between tissue specimens of different types of thyroid carcinomas; Fig. 1 schematically represents the implemented approaches.

In the first approach tissue specimens were compared using an unsupervised approach without any information on the histopathological structure of the samples. Above 200,000 spectra registered for all 15 samples were subjected to a clustering using our own recursive algorithm. Distribution of clusters detected during the deglomerative segmentation was used to estimate general similarities among different tissue samples (Fig. 2A; complete results of the performed segmentation are presented in Supplementary Fig. S1). In the initial analysis all 15 tissue samples were examined together (i.e. global segmentation); clustering (i) in Fig. 2A. Two separate groups of samples were revealed (χ^2 test p-value $< 1e-08$), one of them consisting of medullary cancer (MTC) samples and the other one including all other samples. In the first level of this segmentation the cluster of spectra characteristic for MTC contributed to the majority of all spectra registered for the three MTC samples (89%, 52%, and 58%, respectively) and was negligible in the case of other samples (<1%). The "outlying" MTC samples were removed from subsequent cluster analysis; clustering (ii) in Fig. 2A. This step of deglomerative splitting also revealed two groups of samples (with p-value for overrepresentation $p < 1e-04$): the first group of samples consisted of three samples corresponding to anaplastic carcinoma (ATC), whereas the other group contained all other samples corresponding to differentiated cancer (FTC, PTC-CV and PTC-FV). In the first level of this segmentation the cluster of spectra characteristic for ATC contributed to 61%–97% of all spectra registered for ATC samples, and to 1%–37% of all spectra registered for the remaining samples. For the subsequent analysis the three ATC samples were removed and the next step of deglomerative sample grouping was performed; clustering (iii) in Fig. 2A. However, distributions of clusters in the remaining samples were similar and meaningful discrimination between the types of differentiated cancer was not possible. Furthermore, the contribution of each cluster to the composition of a particular sample was used to classify all 15 tissue specimens. A dendrogram reflecting the similarity of samples based on the distribution of clusters detected at the 3rd level of global segmentation is shown in Fig. 3A. We observed separation of MTC samples and ATC samples in distinct branches of the dendrogram, yet samples corresponding to differentiated cancers were mixed all together. We concluded that the overall features of the samples, which were mirrored in the distribution of clusters detected in a whole specimen, allowed discrimination of the most distinctive types of thyroid cancer — MTC and ATC. However, samples of well-differentiated cancers (FTC, PTC-CV and PTC-FV) cannot be discriminated based on this type of analysis.

In further analyses we implemented additional expert-based information about the location of tissue regions corresponding to tumor. Cancerous regions were identified and marked by a pathologist in

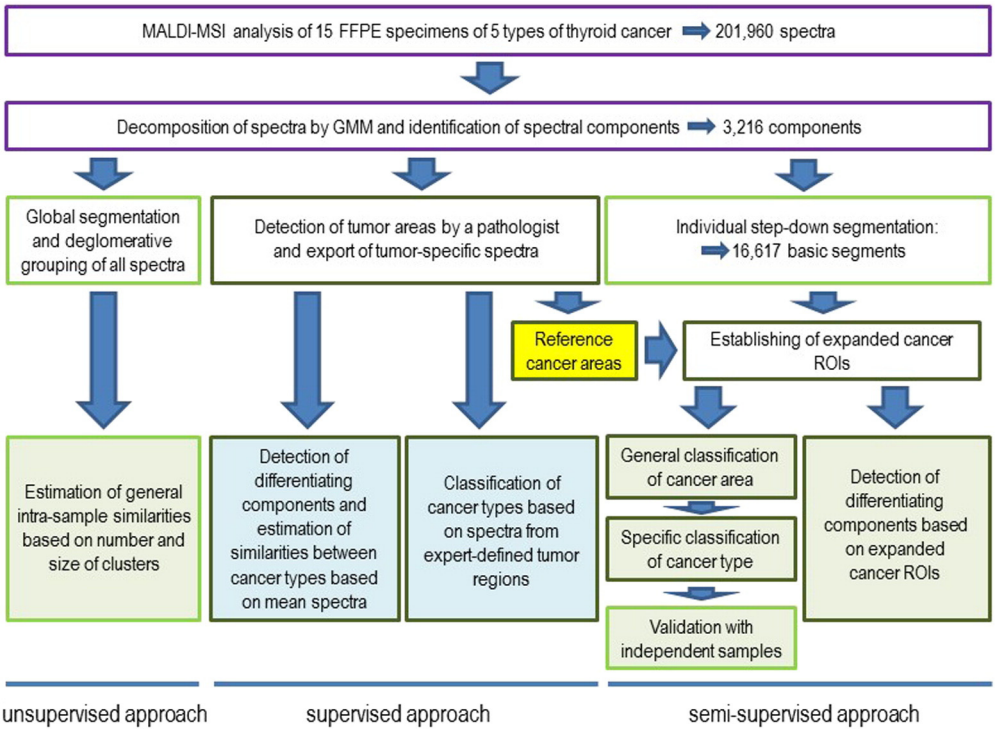

Fig. 1. Different approaches implemented in classification of thyroid cancers.

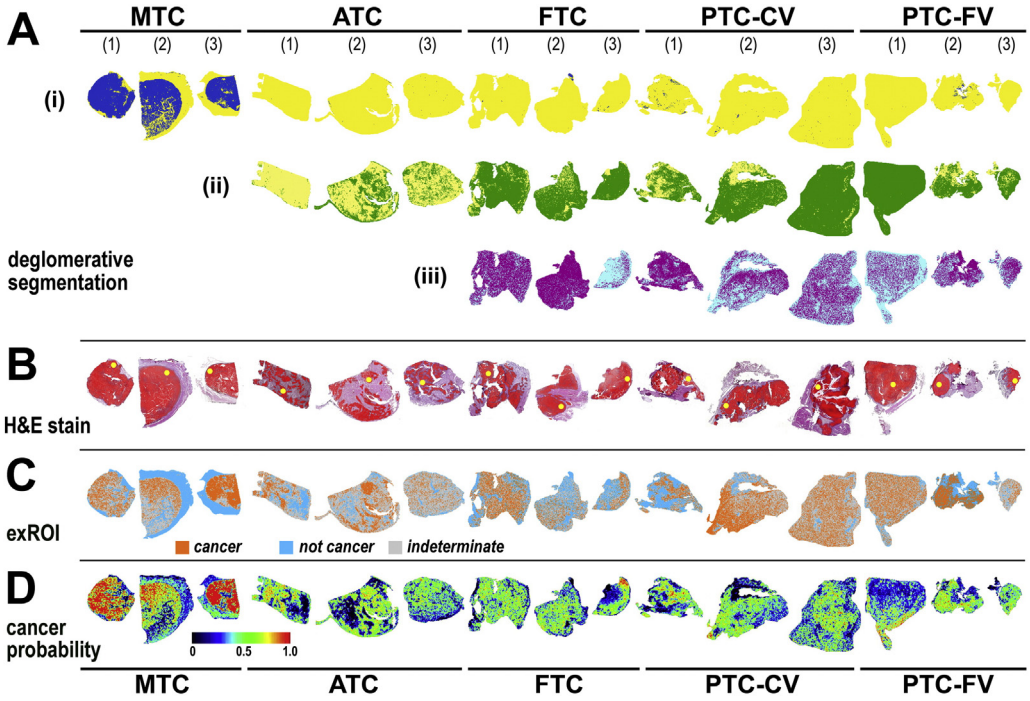

Fig. 2. MALDI-MSI analysis of different types of thyroid cancer. Panel A – Results of the deglomerative grouping of samples. Subsequent clustering experiments (i), (ii) and (iii) were performed for all tissue samples (global segmentation), after removal of MTC samples, and after removal of ATC samples, respectively; marked are clusters detected at the 1st level of segmentation: (i) - yellow and navy blue, (ii) – green and yellow, (iii) – violet and blue. Panel B - Areas corresponding to actual tumor were marked in red on H&E stained tissue preparations; yellow dots correspond to the reference cancer areas. Panel C – Expanded ROIs were established in each sample individually for cancer, not cancer and undefined (indeterminate) areas; only spectra from cancer and not cancer exROIs of samples from the training set were used to train the "cancer versus not cancer" classifier. Panel D – Heatmaps of local cancer probability estimated basing on the general "cancer vs. not cancer" classifier. Abbreviations: MTC – medullary thyroid carcinoma; ATC – anaplastic thyroid carcinoma; FTC – follicular thyroid carcinoma; PTC-CV – papillary thyroid carcinoma, classic variant; PTC-FV – papillary thyroid carcinoma, follicular variant.

each sample (Fig. 2B). Spectra exported from these expert-defined tumor areas (ca. 35–85% of registered spectra) were used for supervised analysis aimed at the identification of components discriminating different types of thyroid cancer; the average tumor-specific spectra computed for each cancer type are presented in Supplementary Fig. S2. First, we tested whether the overall profiles of tumor-related spectra could be used to assess differences between particular types of thyroid malignancies. Vectors of average abundances of GMM-based features were computed for each sample, and then a dendrogram reflecting the detected similarities was calculated by hierarchical agglomeration (Fig. 3B). We observed the separation of MTC samples and ATC samples from samples corresponding to well-differentiated cancers that were present in a separate branch of the dendrogram, yet further separation of the latter samples into specific types was not possible. We hypothesized that potential components having different abundances between the samples of FTC, PTC-CV and PTC-FV were apparently over-dominated by more frequent "non-differentiating" components, hence discrimination of well-differentiated thyroid cancer could not be performed based on a general molecular profile reflected in averaged spectra. However, abundance of components characteristic for MTC and ATC was sufficiently high, which allowed their discrimination also based on general profiles of the registered spectra.

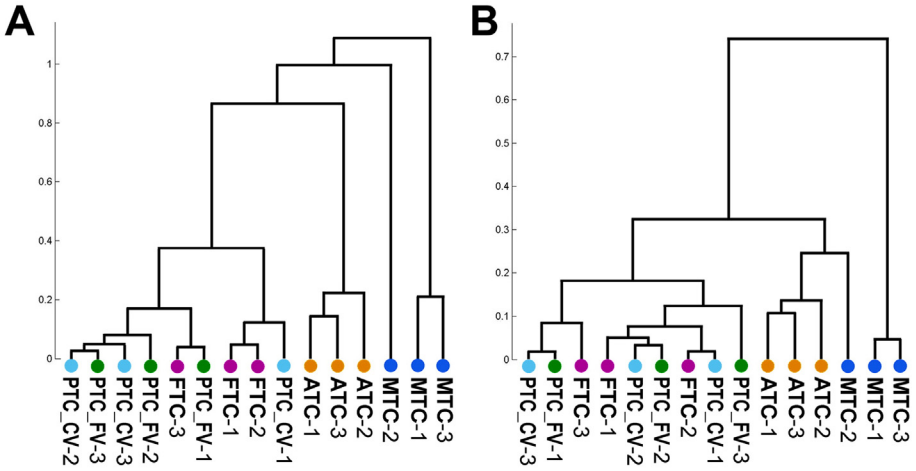

Fig. 3. Similarity between samples corresponding to five different types of thyroid cancer. Panel A – Dendrogram based on general distribution of clusters (at the third level of global segmentation). Panel B – Dendrogram based on average tumor-specific spectra. Abbreviations: MTC – medullary thyroid carcinoma; ATC – anaplastic thyroid carcinoma; FTC – follicular thyroid carcinoma; PTC-CV -papillary thyroid carcinoma, classic variant; PTC-FV – papillary thyroid carcinoma, follicular variant.

Please cite this article as: M. Pietrowska, et al., Molecular profiles of thyroid cancer subtypes: Classification based on features of tissue revealed by mass spectrometry imaging, Biochim. Biophys. Acta (2016), http://dx.doi.org/10.1016/j.bbapap.2016.10.006

To refine the possibility of discrimination of thyroid malignancies based on spectra extracted from expert-defined tumor regions, a classification approach was implemented as the next step. All individual spectra were analyzed using five different "One (cancer type) versus (all) Other (cancer types)" binary classifiers. All 15 tissue samples were split randomly into two sets — a training set (10 specimens; 2 samples from each cancer type) and a testing set (5 specimens; 1 sample from each cancer type). The result of sample classification was considered meaningful if >50% of spectra extracted from tumor area could be assigned to a given type of cancer (an individual spectrum could be classified positively as more than one type, hence the resulting percentages may not add to 100%). We observed reliable classification of all samples in the training set. However, in the testing set only samples of MTC and PTC-FV were classified properly, while the other samples were undetermined (ATC and FTC) or misclassified (PTC-FV); the results are summarized in Table 2.

Moreover, we tested whether molecular features of tissue regions detected by unsupervised segmentation of MSI images could be used for classification of thyroid cancers. For this purpose we implemented a novel method for semi-supervised detection of ROI representing the actual cancer region. For each sample a step-down segmentation was performed that resulted in a large number of small homogeneous clusters (600–1800 clusters per sample), which established "basic segments" and reflected the intrinsic heterogeneity of specimens. Spectra registered in each basic segment were represented by its centroid, which allowed for more than 10-fold reduction in dimensionality (16,617 segments overall) and facilitated further computation. Then, in each specimen a small "reference" region was marked by a pathologist (about 2–4% of the specimen's area) which corresponded to clearly defined foci of cancer cells (excluding necrosis and other tumor-related areas). Similarity of each basic segment to such cancer reference region was assessed afterwards, and subsequently sets of basic segments were identified in each sample individually using a statistical approach: "cancer similar", "not cancer similar" and "indeterminate". Segments in each set were combined to form an expanded ROI (exROI) for cancer, not cancer and unclassified tissue (Fig. 2C). Subsequent classification of cancer types was performed in two steps allowing (i) semi-supervised detection of cancer regions based on general features of thyroid malignancies, and then (ii) identification of cancer types based on features of detected cancer regions only. In the first step, spectra extracted from all cancer exROIs and not cancer exROIs (irrespective of cancer type) were used to test the universal "Cancer vs. Not Cancer" binary classifier, which allowed automated detection of cancer areas in all tissue specimens. The probability of classification of an individual spectrum as cancer-similar is depicted in Fig. 2D in a form of heatmaps; areas containing spectra that showed probability of such classification higher than 50% were considered as actual cancer regions. Afterwards, all individual spectra from cancer regions were analyzed by five "One versus Others" binary classifiers using the same split of samples in the training and the testing set (10 and 5 samples, respectively) as described in the previous section. Positive classification of all samples in the training set was observed (similar to classification based on expert-defined tumor region). In the testing set three samples were classified properly — MTC, ATC and PTC-FV, while two samples were misclassified (FTC and PTC-CV); detailed results are presented in Table 2. This classification approach was further validated using four new independent tissue specimens. In this independent validation set there were two samples classified properly — MTC and ATC, while two samples representing differentiated epithelium-derived cancer (FTC and PTC-CV) were misclassified (Table 2 and Fig. 4). We concluded that the classification approach based on automated detection of expanded cancer ROIs allowed a reliable classification of medullary and anaplastic cancer, which was validated using independent samples. Hence, the results of this innovative approach seemed superior to the results of a more classical approach based on spectra extracted from expert-defined tumor regions. However, this method also failed to discriminate samples of differentiated epithelium-based cancers.

Finally, we searched for spectral components with significantly different abundances between the compared types of thyroid malignancies. The pairwise comparisons were performed between the five types of thyroid cancers (using all 15 samples from the initial sample set) based on spectra from either expert-defined tumor regions or from expanded cancer ROIs described above (detailed results in Supplementary Table S1); examples of such components are presented in Supplementary Fig. S3. As one could expect, the highest number of differentiating components was observed between C-cell-derived and epithelium-derived cancers; about 25% of detected components discriminated MTC from all other types of thyroid cancer. Differences among the types of epithelium-derived cancers were less frequent. There were about 8%, 5% and 2% of detected components that differentiated ATC from both subtypes of PTC, FTC, and all types of differentiated cancers, respectively (in the analysis of spectra from expert-defined

Table 2
Results of cancer type classification performed with classifiers based on expert-defined tumor areas and expanded cancer ROI. Shown is percentage of spectra in cancer regions assigned to a given type of cancer by the "One versus Others" approach. True and false results of classification are marked in bold and italics, respectively.

Sample set	Sample	Classification by expert-defined tumor area						Classification by expanded cancer ROI						Actual type
		MTC	ATC	FTC	PTC_CV	PTC_FV	Result	MTC	ATC	FTC	PTC-CV	PTC-FV	Result	
Training	MTC-1	**99.7%**	1.1%	<0.1%	0.3%	<0.1%	**MTC**	**93.1%**	4.2%	0.2%	0.2%	0.5%	**MTC**	MTC
	MTC-2	**99.6%**	0.2%	0.2%	0.1%	<0.1%	**MTC**	**89.3%**	4.5%	1.6%	2.1%	3.2%	**MTC**	MTC
	ATC-1	0%	**94.1%**	0.3%	0%	<0.1%	**ATC**	<0.1%	**98.1%**	5.8%	1.4%	1.6%	**ATC**	ATC
	ATC-3	0%	**85.1%**	0.4%	9.3%	0.1%	**ATC**	<0.1%	**62.1%**	5.6%	11.1%	6.9%	**ATC**	ATC
	FTC-2	0%	4.8%	**93.9%**	6.5%	0.6%	**FTC**	0.4%	4.2%	**81.3%**	10.9%	2.5%	**FTC**	FTC
	FTC-3	0%	0.4%	**98.4%**	4.6%	12.9%	**FTC**	0%	1.9%	**94.2%**	4.4%	3.5%	**FTC**	FTC
	PTC_CV-1	0.1%	15.4%	7.5%	**82.4%**	5.5%	**PTC_CV**	<0.1%	5.1%	14.4%	**78.4%**	15.7%	**PTC_CV**	PTC_CV
	PTC_CV-2	0%	1.3%	0.2%	**91.6%**	1.2%	**PTC_CV**	<0.1%	5.6%	14.9%	**66.2%**	25.8%	**PTC_CV**	PTC_CV
	PTC_FV-2	0%	1.4%	0.4%	23.6%	**91.6%**	**PTC_FV**	<0.1%	4.1%	6.1%	4.1%	**86.8%**	**PTC_FV**	PTC_FV
	PTC_FV-3	0%	4.4%	0.5%	8.5%	**76.1%**	**PTC_FV**	0%	15.4%	2.3%	11.4%	**71.6%**	**PTC_FV**	PTC_FV
Testing	MTC-3	**98.3%**	0.9%	13.7%	9.4%	0.2%	**MTC**	**56.2%**	6.1%	11.6%	0.4%	3.8%	**MTC**	MTC
	ATC-2	<0.1%	**16.4%**	6.4%	8.9%	0.1%	Undetermined	<0.1%	**57.1%**	33.4%	14.8%	12.9%	**ATC**	ATC
	FTC-1	0%	15.1%	0.5%	31.1%	**35.2%**	Undetermined	0%	11.2%	16.3%	28.3%	**38.4%**	Undetermined	FTC
	PTC_CV-3	0%	<0.1%	23.2%	36.1%	**60.9%**	*PTC_FV*	<0.1%	11.3%	28.7%	33.3%	**66.9%**	*PTC_FV*	PTC_CV
	PTC_FV-1	0%	0%	41.2%	1.4%	**60.3%**	**PTC_FV**	<0.1%	8.8%	74.4%	3.6%	**81.1%**	**PTC_FV**	PTC_FV
Independent validation	V-1							<0.1%	**34.9%**	4.1%	22.1%	17.5%	Undetermined	FTC
	V-2							**50.3%**	7.2%	40.8%	0.6%	18.2%	**MTC**	MTC
	V-3							0%	**54.4%**	3.5%	12.9%	35.4%	*ATC*	PTC_CV
	V-4							0%	**62.7%**	8.4%	5.3%	22.3%	**ATC**	ATC

Please cite this article as: M. Pietrowska, et al., Molecular profiles of thyroid cancer subtypes: Classification based on features of tissue revealed by mass spectrometry imaging, Biochim. Biophys. Acta (2016), http://dx.doi.org/10.1016/j.bbapap.2016.10.006

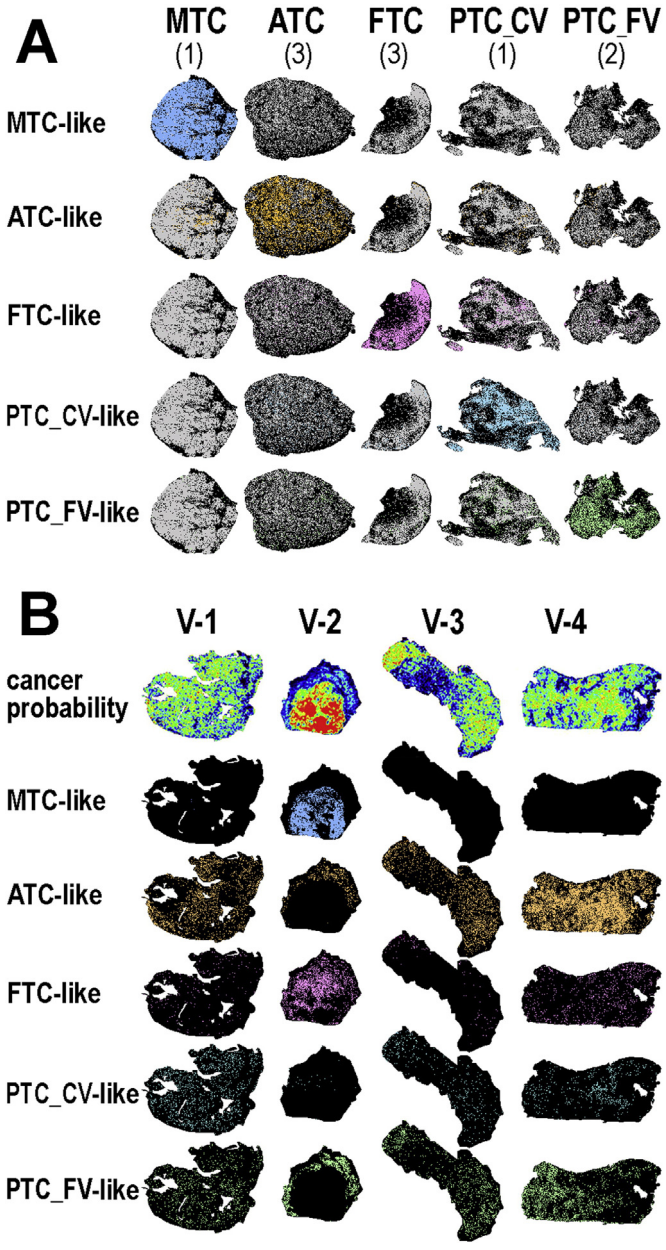

Fig. 4. Results of classification of cancer types by the five "OvO" classifiers using the semi-supervised approach based on exROIs. Panel A – Location of cancer-derived spectra assigned to a particular cancer type in exemplary samples from the training set; samples' areas marked in gray corresponded to cancer exROIs. Panel B – Classification of samples in the independent validation set. Presented are heatmaps of probability of classification of spectra as cancer-derived (upper row, scale the same as in Fig. 2D), and location of cancer-derived spectra assigned to a particular cancer type. Validation samples V-1, V-2, V-3 and V-4 corresponded to FTC, MTC, PTC-CV and ATC, respectively. Abbreviations: MTC – medullary thyroid carcinoma; ATC – anaplastic thyroid carcinoma; FTC – follicular thyroid carcinoma; PTC-CV -papillary thyroid carcinoma, classic variant; PTC-FV – papillary thyroid carcinoma, follicular variant.

tumor areas). Moreover, about 2% of detected components differentiated FTC from both subtypes of PTC. Furthermore, components that discriminated between PTC-CV and PTC-FV were also detected. It is noteworthy that discriminatory components detected in analyses based on spectra from expert-defined tumor areas and from cancer exROIs overlapped substantially (Table 3). Moreover, the analysis based on exROIs reduced unexpectedly large difference between samples of PTC-FV and all remaining samples, observed in spectra from expert-defined areas, which made subsequent comparisons more credible.

4. Discussion

One of the major advantages of MALDI-MSI lies in its capability to measure abundances of molecular species in the histological context. This approach allows unbiased analysis of intact tissue sections, avoiding sample homogenization and preserving its anatomical features. As a result molecular information specific for particular tissue regions can be revealed without the necessity of their physical separation. Moreover, the ability to perform unsupervised analysis of imaging data allows the discrimination of tissue regions which could not be revealed by classical morphology-based approaches [30–36]. Complex composition of tissues and organs results in the possible "contamination" of a target of interest with products of adjacent or intruding tissues, which is a potential problem in many types of molecular studies. Therefore, a study focused specifically on cancer proteome could be challenged by the necessity of the physical separation of cancer cells from other tissue components such as necrotic areas, connective tissue or muscles by using laser microdissection to provide the best quality of results [52]. In this study the MALDI-MSI approach was used to search for molecular features characteristic for different types of thyroid malignancies. Molecular signatures of cancer were established using spectra exported from specific tissue areas defined by a pathologist as a tumor based on their morphological features, which might be called a "virtual microdissection". Precise combination of a molecular profile with its histological context requires annotation of MSI data with a morphological picture using the same section of FFPE material. However, histological inspection of H&E stained tissue follows MALDI-MSI, hence microscopically analyzed material is potentially damaged and distorted by earlier procedures. Moreover, cancer cells could form micro-foci embedded within other types of cells or may have morphology resembling normal tissue. As a consequence, some details of cancerous tissue structure could be missed or improperly interpreted during a pathologist re-inspection of tissue samples previously subjected to MALDI-MSI. To overcome this potential problem we propose an approach that combines expert knowledge and unsupervised segmentation of MSI maps. A small "reference" cancer area is detected by the pathologist that contains actual cancer cells and is devoid of necrotic cells and components of tumor niche. The whole tissue specimen is subjected to in-depth segmentation which allows us to detect small homogenous clusters, called "basic segments", which reflect the intrinsic heterogeneity of tissue. Then, basic segments showing a high degree of molecular (spectral) similarity to the cancer reference area are detected and merged as a "cancer extended ROI" to be used in further analyses. This semi-supervised approach helped retrieve information from small foci of the cancer cell and to use all spectra potentially reflecting molecular features of cancer. Simultaneously, confounding information related to small foci of normal or necrotic cells frequently intruding into the cancer area was removed. Moreover, our approach offers other important benefits, which include substantial dimension reduction in large datasets resulting in lower computation load required for their analyses, as well as less laborious and more credible work of an expert in detection of specific areas present in a heterogeneous tissue specimen. Hence, universal merits of the proposed approach make it useful for any other MSI-based study oriented on detection and characterization of disease-affected tissue regions.

In this work molecular profiles of tissue sub-regions revealed by supervised, semi-supervised and unsupervised analyses of MALDI-MSI data were used aiming to classify different types of thyroid cancers. All implemented approaches allowed the reliable discrimination of samples containing medullary thyroid carcinoma. MTC is a thyroid malignancy uniquely derived from neuroendocrine parafollicular C-cells. Its molecular profile is apparently distinct from other thyroid malignancies derived from follicular epithelial cells, and includes expression of calcitonin and other hormone-related proteins [53]. The abundance of molecular factors characteristic for MTC appeared sufficient to allow detection of this type of cancer based on the results of unsupervised segmentation of MSI-generated data, as well as for proper classification of

Please cite this article as: M. Pietrowska, et al., Molecular profiles of thyroid cancer subtypes: Classification based on features of tissue revealed by mass spectrometry imaging, Biochim. Biophys. Acta (2016), http://dx.doi.org/10.1016/j.bbapap.2016.10.006

Table 3
Number of spectral components with significantly different abundances between areas corresponding to different types of thyroid cancer. Each line with bolded characters represents the number of differentiating components which overlapped in pairwise comparison listed in the lines above.

Difference between cancer types	Number of discriminating components		
	Expert-defined cancer areas	Expanded cancer ROI	Both criteria
MTC vs. ATC	1581 (49%)	1868 (58%)	1548 (48%)
MTC vs. FTC	1995 (62%)	2040 (64%)	1892 (59%)
MTC vs. PTC-CV	1639 (51%)	1759 (55%)	1572 (49%)
MTC vs. PTC-FV	1792 (56%)	1770 (55%)	1595 (50%)
MTC vs. all no-MTC	**804 (25%)**	**1108 (34%)**	**757 (24%)**
ATC vs. PTC-CV	300 (9,3%)	275 (8.6%)	215 (6.7%)
ATC vs. PTC-FV	1927 (59%)	663 (21%)	643 (20%)
ATC vs. all PTC	**258 (8.0%)**	**241 (7.5%)**	**179 (5.6%)**
ATC vs. FTC	171 (5.3%)	80 (2.5%)	73 (2.3%)
ATC vs. all no-ATC	**73 (2.3%)**	**53 (1.7%)**	**40 (1.2%)**
FTC vs. PTC-CV	85 (2.6%)	103 (3.2%)	60 (1.9%)
FTC vs. PTC-FV	1342 (42%)	405 (13%)	389 (12%)
FTC vs. all PTC	55 (1.7%)	92 (2.9%)	**50 (1.6%)**
PTC-CV vs. PTC-FV	1182 (37%)	77 (2.4%)	72 (2.2%)

Abbreviations: MTC — medullary thyroid carcinoma; ATC — anaplastic thyroid carcinoma; FTC — follicular thyroid carcinoma; PTC-CV — papillary thyroid carcinoma, classic variant; and PTC-FV — papillary thyroid carcinoma, follicular variant.

this malignancy validated with independent samples. This is a meaningful observation because MTC frequently represents a follicular pattern of growth, hence its histopathological examination should be frequently supplemented with molecular diagnostics for proper discrimination from epithelium-derived follicular tumors [54]. Another type of thyroid cancer that could be discriminated thanks to the analysis of MALDI-MSI data was undifferentiated anaplastic cancer (ATC), which was separated from differentiated cancers based on distribution of the detected clusters as well as general composition of its molecular profile (i.e. average spectrum registered by MALDI-MSI). Moreover, proper classification of this malignancy was also validated with independent samples. Significant differences in proteomic profiles between undifferentiated and differentiated thyroid carcinomas could be predicted based on robust differences in gene expression profiles among these malignancies, which apparently involves dysregulation of matrix metalloproteinase pathways in ATC [55]. On the other hand, analyses based on molecular profiles detected during MALDI-MSI could neither discriminate nor classify three types of differentiated thyroid carcinomas. However, it should be noted that histopathological diagnosis of PTC-CV, PTC-FV and FTC is strictly based on microscopic examination of tissue morphology (e.g. structure of cell nuclei) [5,9]. Relatively low spatial resolution of MALDI-MSI used in the present study (100 μm) did not allow the addressing of microscopic features of tissues. This limitation, together with the relative similarity of general molecular profiles detected by MALDI-MSI in differentiated thyroid cancers, could contribute to the low discriminatory power of the classification methods used in the present work. However, the feasibility of classification of thyroid malignancies using MSI analysis of tissue specimens might be reassessed if methods based on molecular profiles used data recorded with a higher spatial resolution or were combined with approaches addressing the texture of samples.

Molecular differences between differentiated thyroid carcinomas – papillary and follicular – were observed at the level of gene expression profiles [21] and cancer metabolome [15]. Moreover, differences between PTC and FTC were also reported at the level of cancer proteome. A set of 9 proteins isolated from tissue extracts, including 14-3-3 isoforms, ANXA5, TUBA1B, PRX6, A1AT, SELENBP1, and PDIp, could discriminate PTC and FTC with 100% positive predictive value [26]. However, proteomic signatures specific for classical and follicular variants of PTC, which could support differential diagnosis of these two variants of papillary cancer, were not reported. The MALDI-MSI approach was previously applied to analyze cytological smears of FNA thyroid specimens. There were several spectral components revealed that discriminated different types of thyroid tumors: benign nodules, Hurthle cell follicular adenomas, PTC and MTC [45–47]. Moreover, a few spectral components discriminating classical and follicular variants of PTC were also detected using cytological material [46]. Here we found that analysis of spectra exported from tumor regions allowed detection of several components with significantly different abundances between FTC, PTC-CV and PTC-FV. We concluded that MALDI-MSI that allows retrieval of molecular profiles specific for tumor regions, which could be called "virtual microdissection", followed by the identification of differentiating proteins by on-tissue MS/MS is a promising approach to detect potential biomarkers to support diagnosis of differentiated thyroid tumors.

Supplementary data to this article can be found online at doi:10.1016/j.bbapap.2016.10.006.

Funding sources

This work was supported by the National Science Centre, Poland, Grant 2012/07/B/NZ4/01450 (to PW) and Grant 2015/19/B/ST6/01736 (to JP), and the National Centre for Research and Development, Poland, Grant DZP/STATEGMED2/2554/2014. The computations were carried out using the GeCONil infrastructure (Grant POIG.02.03.01-24-099). The cooperative work was performed in the frame of the EU BMBS COST Action BM1104.

Transparency document

The Transparency document associated with this article can be found, in the online version.

References

[1] R.L. Siegel, K.D. Miller, A. Jemal, Cancer statistics, 2015, CA Cancer J. Clin. 65 (1) (2015) 5–29, http://dx.doi.org/10.3322/caac.21254.
[2] G.B. Salabè, Pathogenesis of thyroid nodules: histological classification? Biomed. Pharmacother. 55 (1) (2001) 39–53.
[3] R.A. DeLellis, R.V. Lloyd, P.U. Heitz, C. Eng, Pathology and Genetics of Tumours of Endocrine Organs. WHO Classification of Tumours, IARC Press, Lyon, 2004.
[4] Y.C. Oertel, Classification of Thyroid Malignancies, in: L. Wartofsky, D. Van Nostrand (Eds.), Thyroid Cancer: A Comprehensive Guide to Clinical Management, Human Press, New Jersey 2004, pp. 85–87.
[5] C. Hedinger, E.D. Williams, L.H. Sobin, Histological typing of thyroid tumors, International Histological Classification of Tumours, 2nd ed., 11, Springer-Verlag, Berlin, 1988.
[6] G.H. Sakorafas, Thyroid nodules; interpretation and importance of fine-needle aspiration (FNA) for the clinician — practical considerations, Surg. Oncol. 19 (4) (2010) 130–139, http://dx.doi.org/10.1016/j.suronc.2010.06.003.
[7] K. Kakudo, K. Kameyama, A. Miyauchi, H. Nakamura, Introducing the reporting system for thyroid fine-needle aspiration cytology according to the new guidelines of the Japan Thyroid Association, Endocr. J. 61 (6) (2014) 539–552.
[8] W.C. Faquin, The thyroid gland: recurring problems in histologic and cytologic evaluation, Arch Pathol Lab Med. 132 (4) (2008) 622–632 (doi:10.1043/1543–2165(2008)132[622:TTGRPI]2.0.CO; 2).
[9] M. Schlumberger, Papillary and follicular thyroid carcinoma, Ann Endocrinol. (Paris) 68 (2007) 120–128.
[10] B. Ustun, D. Chhieng, M.L. Prasad, E. Holt, L. Hammers, T. Carling, R. Udelsman, A.J. Adeniran, Follicular variant of papillary thyroid carcinoma: accuracy of FNA diagnosis and implications for patient management, Endocr. Pathol. 25 (3) (2014) 257–264, http://dx.doi.org/10.1007/s12022-014-9301-3.
[11] M. Eszlinger, R. Paschke, Molecular fine-needle aspiration biopsy diagnosis of thyroid nodules by tumor specific mutations and gene expression patterns, Mol. Cell. Endocrinol. 322 (1–2) (2010) 29–37, http://dx.doi.org/10.1016/j.mce.2010.01.010.
[12] K. Krause, B. Jessnitzer, D. Fuhrer, Proteomics in thyroid tumor research, J. Clin. Endocrinol. Metab. 94 (8) (2009) 2717–2724, http://dx.doi.org/10.1210/jc.2009-0308.
[13] P. Aragon Han, M.T. Olson, R. Fazeli, J.D. Prescott, S.I. Pai, E.B. Schneider, R.P. Tufano, M.A. Zeiger, The impact of molecular testing on the surgical management of patients with thyroid nodules, Ann. Surg. Oncol. 21 (6) (2014) 1862–1869, http://dx.doi.org/10.1245/s10434-014-3508-x.
[14] O.L. Griffith, C.G. Chiu, A.M. Gown, S.J. Jones, S.M. Wiseman, Biomarker panel diagnosis of thyroid cancer: a critical review, Expert. Rev. Anticancer. Ther. 8 (9) (2008) 1399–1413, http://dx.doi.org/10.1586/14737140.8.9.1399.
[15] A. Wojakowska, M. Chekan, P. Widłak, M. Pietrowska, Application of metabolomics in thyroid cancer research, Int. J. Endocrinol. 2015 (2015) 258763, http://dx.doi.org/10.1155/2015/258763.

[16] F. Pagni, V. L'Imperio, F. Bono, M. Garancini, G. Roversi, G. De Sio, M. Galli, A.J. Smith, C. Chinello, F. Magni, Proteome analysis in thyroid pathology, Expert Rev. Proteomics 12 (4) (2015) 375–390, http://dx.doi.org/10.1586/14789450.2015.1062369.
[17] Cancer Genome Atlas Research Network, Integrated genomic characterization of papillary thyroid carcinoma, Cell 159 (3) (2014 Oct 23) 676–690, http://dx.doi.org/10.1016/j.cell.2014.09.050.
[18] B. Jarzab, M. Wiench, K. Fujarewicz, K. Simek, M. Jarzab, M. Oczko-Wojciechowska, J. Wloch, A. Czarniecka, E. Chmielik, D. Lange, A. Pawlaczek, S. Szpak, E. Gubala, A. Swierniak, Gene expression profile of papillary thyroid cancer: sources of variability and diagnostic implications, Cancer Res. 65 (4) (2005) 1587–1597.
[19] K. Fujarewicz, M. Jarzab, M. Eszlinger, K. Krohn, R. Paschke, M. Oczko-Wojciechowska, M. Wiench, A. Kukulska, B. Jarzab, A. Swierniak, A multi-gene approach to differentiate papillary thyroid carcinoma from benign lesions: gene selection using support vector machines with bootstrapping, Endocr. Relat. Cancer. 14 (3) (2007) 809–826, http://dx.doi.org/10.1677/ERC-06-0048.
[20] T.J. Giordano, R. Kuick, D.G. Thomas, D.E. Misek, M. Vinco, D. Sanders, Z. Zhu, R. Ciampi, M. Roh, K. Shedden, P. Gauger, G. Doherty, N.W. Thompson, S. Hanash, R.J. Koenig, Y.E. Nikiforov, Molecular classification of papillary thyroid carcinoma: distinct BRAF, RAS, and RET/PTC mutation-specific gene expression profiles discovered by DNA microarray analysis, Oncogene 24 (44) (2005) 6646–6656.
[21] M. Eszlinger, K. Krohn, A. Kukulska, B. Jarzab, R. Paschke, Perspectives and limitations of microarray-based gene expression profiling of thyroid tumors, Endocr. Rev. 28 (3) (2007) 322–338.
[22] L.M. Brown, S.M. Helmke, S.W. Hunsucker, R.T. Netea-Maier, S.A. Chiang, D.E. Heinz, K.R. Shroyer, M.W. Duncan, B.R. Haugen, Quantitative and qualitative differences in protein expression between papillary thyroid carcinoma and normal thyroid tissue, Mol. Carcinog. 45 (8) (2006) 613–626.
[23] Y. Ban, G. Yamamoto, M. Takada, S. Hayashi, Y. Ban, K. Shimizu, H. Akasu, T. Igarashi, Y. Bando, T. Tachikawa, T. Hirano, Proteomic profiling of thyroid papillary carcinoma, J. Thyroid. Res. 815079 (2012), http://dx.doi.org/10.1155/2012/815079.
[24] R.T. Netea-Maier, S.W. Hunsucker, B.M. Hoevenaars, S.M. Helmke, P.J. Slootweg, A.R. Hermus, B.R. Haugen, M.W. Duncan, Discovery and validation of protein abundance differences between follicular thyroid neoplasms, Cancer Res. 68 (5) (2008) 1572–1580, http://dx.doi.org/10.1158/0008-5472.CAN-07-5020.
[25] E. Uyy, V.I. Suica, R.M. Boteanu, D. Manda, A.E. Baciu, C. Badiu, F. Antohe, Endoplasmic reticulum chaperones are potential active factors in thyroid tumorigenesis, J. Proteome Res. 15 (9) (2016) 3377–3387, http://dx.doi.org/10.1021/acs.jproteome.6b00567.
[26] A. Sofiadis, S. Becker, U. Hellman, L. Hultin-Rosenberg, A. Dinets, M. Hulchiy, J. Zedenius, G. Wallin, T. Foukakis, A. Höög, G. Auer, J. Lehtiö, C. Larsson, Proteomic profiling of follicular and papillary thyroid tumors, Eur. J. Endocrinol. 166 (4) (2012) 657–667, http://dx.doi.org/10.1530/EJE-11-0856.
[27] A. Wojakowska, M. Chekan, Ł. Marczak, K. Polanski, D. Lange, M. Pietrowska, P. Widlak, Detection of metabolites discriminating subtypes of thyroid cancer: molecular profiling of FFPE samples using the GC/MS approach, Mol. Cell. Endocrinol. 417 (2015) 149–157, http://dx.doi.org/10.1016/j.mce.2015.09.021.
[28] K.M. Denning, P.C. Smyth, S.F. Cahill, S.P. Finn, E. Conlon, J. Li, R.J. Flavin, S.T. Aherne, S.M. Guenther, A. Ferlinz, J.J. O'Leary, O.M. Sheils, A molecular expression signature distinguishing follicular lesions in thyroid carcinoma using preamplification RT-PCR in archival samples, Mod. Pathol. 20 (10) (2007) 1095–1102.
[29] S. Le Pennec, T. Konopka, D. Gacquer, D. Fimereli, M. Tarabichi, G. Tomás, F. Savagner, M. Decaussin-Petrucci, C. Trésallet, G. Andry, D. Larsimont, V. Detours, C. Maenhaut, Intratumor heterogeneity and clonal evolution in an aggressive papillary thyroid cancer and matched metastases, Endocr Relat Cancer 22 (2) (2015) 205–216, http://dx.doi.org/10.1530/ERC-14-0351.
[30] R.L. Caldwell, R.M. Caprioli, Tissue profiling by mass spectrometry: a review of methodology and applications, Mol. Cell. Proteomics 4 (2005) 394–401.
[31] D.S. Cornett, M.L. Reyzer, P. Chaurand, R.M. Caprioli, MALDI imaging mass spectrometry: molecular snapshots of biochemical systems, Nat. Methods 4 (2007) 828–833.
[32] L.A. McDonnell, R.M.A. Heeren, Imaging mass spectrometry, Mass Spectrom. Rev. 26 (2007) 606–643.
[33] E.H. Seeley, R.M. Caprioli, MALDI imaging mass spectrometry of human tissue: method challenges and clinical perspectives, Trends Biotechnol. 29 (2011) 136–143, http://dx.doi.org/10.1016/j.tibtech.2010.12.002.
[34] M. Aichler, A. Walch, MALDI imaging mass spectrometry: current frontiers and perspectives in pathology research and practice, Lab. Investig. 95 (2015) 422–431, http://dx.doi.org/10.1038/labinvest.2014.156.
[35] K. Schwamborn, R.M. Caprioli, Molecular imaging by mass spectrometry — looking beyond classical histology, Nat. Rev. Cancer 10 (2010) 639–646, http://dx.doi.org/10.1038/nrc2917.
[36] C. Schöne, H. Höfler, A. Walch, MALDI imaging mass spectrometry in cancer research: combining proteomic profiling and histological evaluation, Clin. Biochem. 46 (2013) 539–545, http://dx.doi.org/10.1016/j.clinbiochem.2013.01.018.
[37] S. Meding, U. Nitsche, B. Balluff, M. Elsner, S. Rauser, C. Schöne, M. Nipp, M. Maak, M. Feith, M.P. Ebert, H. Friess, R. Langer, H. Höfler, H. Zitzelsberger, R. Rosenberg, A. Walch, Tumor classification of six common cancer types based on proteomic profiling by MALDI imaging, J. Proteome Res. 11 (3) (2012 Mar 2) 1996–2003, http://dx.doi.org/10.1021/pr200784p.
[38] R.F. Oezdemir, N.T. Gaisa, K. Lindemann-Docter, S. Gostek, R. Weiskirchen, M. Ahrens, K. Schwamborn, C. Stephan, D. Pfister, A. Heidenreich, R. Knuechel, C. Henkel, Proteomic tissue profiling for the improvement of grading of noninvasive papillary urothelial neoplasia, Clin. Biochem. 45 (1–2) (2012 Jan) 7–11, http://dx.doi.org/10.1016/j.clinbiochem.2011.09.013.
[39] B. Balluff, F. C.K., M. S.K., C. Schöne, B. Kuster, M. Schmitt, M. Aubele, H. Höfler, D. A.M., A. Heck Jr., H. P.C., J. Morreau, M.A. A.F., A. Walch, M.D. L.A., De novo discovery of phenotypic intratumour heterogeneity using imaging mass spectrometry, J. Pathol. 235 (2015) 3–13, http://dx.doi.org/10.1002/path.4436.
[40] T. Alexandrov, M. Becker, O. Guntinas-Lichius, G. Ernst, F. von Eggeling, MALDI-imaging segmentation is a powerful tool for spatial functional proteomic analysis of human larynx carcinoma, J. Cancer Res. Clin. Oncol. 139 (2013) 85–95, http://dx.doi.org/10.1007/s00432-012-1303-2.
[41] R.L. Caldwell, A. Gonzalez, S.R. Oppenheimer, S. H.S., R.M. Caprioli, Molecular assessment of the tumor protein microenvironment using imaging mass spectrometry, Cancer Genomics Proteomics 3 (2006) 279–288.
[42] R.S. Oppenheimer, D. Mi, M.E. Sanders, R.M. Caprioli, Molecular analysis of tumor margins by MALDI mass spectrometry in renal carcinoma, J. Proteome Res. 9 (2010) 2182–2190, http://dx.doi.org/10.1021/pr900936z.
[43] S. Kang, S. H.S., L. J.S., K. D.S., K. H.Y., H. S.H., K. P.S., Y. J.H., C. N.H., Molecular proteomics imaging of tumor interfaces by mass spectrometry, J. Proteome Res. 9 (2010) 1157–1164, http://dx.doi.org/10.1021/pr900666q.
[44] J. E.A., N. Schmitz, W. C.J., F. C.K., A. van Remoortere, v.Z. R.J., H. A.J., H. P.C., D. A.M., A. A.F., B. J.V., L.A. McDonnell, Imaging mass spectrometry-based molecular histology differentiates microscopically identical and heterogeneous tumors, J. Proteome Res. 12 (2013) 1847–1855, http://dx.doi.org/10.1021/pr301190g.
[45] V. Mainini, F. Pagni, M. Garancini, V. Giardini, G. De Sio, C. Cusi, C. Arosio, G. Roversi, C. Chinello, P. Caria, R. Vanni, F. Magni, An alternative approach in endocrine pathology research: MALDI-IMS in papillary thyroid carcinoma, Endocr. Pathol. 24 (2013) 250–253, http://dx.doi.org/10.1007/s12022-013-9273-8.
[46] F. Pagni, V. Mainini, M. Garancini, F. Bono, A. Vanzati, V. Giardini, M. Scardilli, P. Goffredo, A.J. Smith, M. Galli, G. De Sio, F. Magni, Proteomics for the diagnosis of thyroid lesions: preliminary report, Cytopathology 26 (5) (2015) 318–324, http://dx.doi.org/10.1111/cyt.12166.
[47] F. Pagni, G. De Sio, M. Garancini, M. Scardilli, C. Chinello, A.J. Smith, F. Bono, D. Leni, F. Magni, Proteomics in thyroid cytopathology: relevance of MALDI-imaging in distinguishing malignant from benign lesions, Proteomics (2016 Mar 31), http://dx.doi.org/10.1002/pmic.201500448.
[48] K.W. Min, J.Y. Bang, K.P. Kim, W.S. Kim, S.H. Lee, S.R. Shanta, J.H. Lee, J.H. Hong, S.D. Lim, Y.B. Yoo, C.H. Na, Imaging mass spectrometry in papillary thyroid carcinoma for the identification and validation of biomarker proteins, J. Korean Med. Sci. 29 (7) (2014) 934–940, http://dx.doi.org/10.3346/jkms.2014.29.7.934.
[49] A. Polanski, M. Marczyk, M. Pietrowska, P. Widlak, J. Polanska, Signal partitioning algorithm for highly efficient Gaussian mixture modeling in mass spectrometry, PLoS ONE 10 (7) (2015) e0134256, http://dx.doi.org/10.1371/journal.pone.0134256.
[50] P. Widlak, G. Mrukwa, M. Kalinowska, M. Pietrowska, M. Chekan, J. Wierzgon, M. Gawin, G. Drazek, J. Polanska, Detection of molecular signatures of oral squamous cell carcinoma and normal epithelium — application of a novel methodology for unsupervised segmentation of imaging mass spectrometry data, Proteomics 16 (11-12) (2016) 1613–1621, http://dx.doi.org/10.1002/pmic.201500458.
[51] M. Marczyk, R. Jaksik, A. Polanski, J. Polanska, Adaptive filtering of microarray gene expression data based on Gaussian mixture decomposition, BMC Bioinformatics 14 (2013) 101, http://dx.doi.org/10.1186/1471-2105-14-101.
[52] J.R. Wisniewski, K. Dus, M. Mann, Proteomic workflow for analysis of archival formalin-fixed and paraffin-embedded clinical samples to a depth of 10 000 proteins, Proteomics Clin. Appl. 7 (2013) 225–233, http://dx.doi.org/10.1002/prca.201200046.
[53] R.V. Lloyd, J.C. Sisson, P.J. Marangos, Calcitonin, carcinoembryonic antigen and neuron-specific enolase in medullary thyroid carcinoma, Cancer 51 (1983) 2234–2239.
[54] Cakir M, Altunbas H, Balci MK, Karayalcin U, Karpuzoglu G. Medullary thyroid carcinoma, follicular variant. Endocr Pathol, 2002; 13(1):75–79.
[55] J. Espinal-Enríquez, S. Muñoz-Montero, I. Imaz-Rosshandler, A. Huerta-Verde, C. Mejía, E. Hernández-Lemus, Genome-wide expression analysis suggests a crucial role of dysregulation of matrix metalloproteinases pathway in undifferentiated thyroid carcinoma, BMC Genomics 16 (2015) 207, http://dx.doi.org/10.1186/s12864-015-1372-0.

Please cite this article as: M. Pietrowska, et al., Molecular profiles of thyroid cancer subtypes: Classification based on features of tissue revealed by mass spectrometry imaging, Biochim. Biophys. Acta (2016), http://dx.doi.org/10.1016/j.bbapap.2016.10.006